Engineering Geology 238 (2018) 1–14

Contents lists available at ScienceDirect

Engineering Geology

journal homepage: www.elsevier.com/locate/enggeo

# Application of an ultra-wide band sensor-free wireless network for ground monitoring

Emanuele Intrieri[a,*], Giovanni Gigli[a], Teresa Gracchi[a], Massimiliano Nocentini[a], Luca Lombardi[a], Francesco Mugnai[a], William Frodella[a], Giovanni Bertolini[b], Ennio Carnevale[c], Massimiliano Favalli[d], Alessandro Fornaciai[d], Jordi Marturià Alavedra[e], Lorenzo Mucchi[c], Luca Nannipieri[d], Xavier Rodriguez-Lloveras[e], Marco Pizziolo[b], Rosa Schina[f], Federico Trippi[f], Nicola Casagli[a]

[a] Department of Earth Sciences, University of Florence, via La Pira 4, 50121 Florence, Italy
[b] Agency for Territorial Safety and Civil Protection, Emilia-Romagna Region, via Emilia Santo Stefano 25, 42100 Reggio Emilia, Italy
[c] Department of Information Engineering, University of Florence, via di Santa Marta 3, 50139 Florence, Italy
[d] INGV (National Institute of Geophysics and Volcanology), via della Faggiola 32, 56126 Pisa, Italy
[e] ICGC (Institut Cartogràfic i Geològic de Catalunya), Parc de Montjuïc, 08038 Barcelona, Spain
[f] International Consortium for Advanced Design, via di Santa Marta 3, 50139 Florence, Italy

ARTICLE INFO

*Keywords:*
Wireless sensor network
Slope stability
Subsidence
Early warning
Monitoring

ABSTRACT

Ground displacement monitoring is one of the most important aspects of early warning systems and risk management strategies when addressing phenomena such as landslides or subsidence. Several types of instrumentation already exist, but those able to provide real-time warnings on multiple time series are typically based on expensive technology, highlighting the need to develop a low-cost, easy to install system suitable for emergency monitoring. Therefore, a wireless network based on ultra-wideband impulse radiofrequency technology has been realized. The novelty of this network consists of its ability to measure the distance between nodes using the same signals used for transmission without the need for an actual measurement sensor. The system was tested by monitoring a mudflow in Central Italy and revealed its suitability as an early warning tool. More research on the integration of future low-cost hardware and eventual industrialization would provide further improvement to this promising technology.

## 1. Introduction

The current technological level and the actual need for risk reduction strategies have led to the development of many instruments for monitoring ground movement, including both slope instability and subsidence. For a thorough dissertation of these instruments, several literature reviews that provide details about their function and application are available (Casagli et al., 2017; Dunnicliff, 1993, 1995; Read and Stacey, 2009; Vaziri et al., 2010). A study of the state-of-the-art instrumentation revealed that among the most commonly used and versatile instruments, there was a lack of a low-cost, easy to install tool suitable for emergency monitoring, i.e. for those situations where the priority is to rapidly gather preliminary information concerning the kinematics of a slope in order to help decision makers.

For example, robotic total stations (RTSs) enable measurements of the distance and vertical and horizontal angles, making it possible to retrieve the absolute position of a target and, therefore, its displacement. Modern systems can operate automatically with high acquisition frequency and millimeter precision (Giordan et al., 2013; Liu et al., 2004; Mantovani et al., 2000; Rizzo and Leggeri, 2004; Petley et al., 2005). The disadvantages of this technique include the high cost and the need for a clear line of sight (LOS) between the target (usually a prism) and the station.

In contrast, GNSS systems do not require a LOS and are capable of providing high-precision 3D monitoring. However, the cost of a single antenna makes it difficult to monitor more than a few control points, especially if the movements of a landslide cause disruption of the device. A detailed study of the application of GNSS to landslides can be found in Gili et al. (2000) and examples of application in Malet et al. (2002), Mora et al. (2003), Squarzoni et al. (2005). In recent years, the development of low-cost GNSS equipment provided new possibilities for the application of such technology to landslides (Günther et al.,

* Corresponding author.
*E-mail address:* emanuele.intrieri@unifi.it (E. Intrieri).

https://doi.org/10.1016/j.enggeo.2018.02.017
Received 30 March 2017; Received in revised form 22 January 2018; Accepted 22 February 2018
Available online 01 March 2018

2008; Heunecke et al., 2011; Cina and Piras, 2015).

Ground-based interferometric Synthetic Aperture Radar (GB-InSAR) is one of the best performing landslide monitoring instruments due to its ability to produce 2D displacement maps, and it has established itself as the best practice in open-pit mine monitoring (Farina et al., 2011; Read and Stacey, 2009; Severin et al., 2014). Furthermore, this tool can achieve mm precision and can be adopted within an early warning system (Intrieri et al., 2012; Gigli et al., 2014; Lombardi et al., 2017). GB-InSAR has also been employed to detect subsidence preceding sinkhole collapse (Intrieri et al., 2015). Nevertheless, this technique has some major limitations, such as the high cost and the capability to measure only the movement component parallel to the instrument LOS.

In this context, the aim was to develop a novel, low-cost, easy to install monitoring system, Wi-GIM (standing for Wireless Ground Instability Monitoring) to perform real-time ground displacement measurements to provide early warning.

## 2. Materials and methods: Wi-GIM architecture and technology

Wireless sensor network (WSN) technology has the capability to quickly capture, process, and transmit data real-time. After deployment in the environment, wireless sensors create a network by inter-connecting to each other. This network of sensors has the advantage of being highly flexible and easy to install: sensors can be distributed as needed and adapted to the environment. This fulfils an important need for real-time monitoring, especially in hazardous or remote conditions. However, WSN has its own limitations. The sensors have size constraints, which means they cannot be very complex with respect to both hardware and software. Additionally, they typically cannot carry large amounts of battery power.

The WSNs in literature (Fernández-Steeger et al., 2009; Garich, 2007; Hill and Sippel, 2002; Kotta et al., 2011; Kung et al., 2006; Ohbayashi et al., 2008; Ramesh et al., 2009; Rosi et al., 2011; Sheth et al., 2005; Terzis et al., 2006) mainly exploit radiofrequency signals to provide connectivity to the sensor nodes not to measure the distance between nodes. In contrast, the Wi-GIM system presented in this paper is aimed at using a particular WSN in a landslide scenario in order to estimate its deformational field. This is achieved by using an impulsive radiofrequency technology, such as ultra-wideband (UWB), to measure the distance between nodes of a WSN, thus creating a “grid” over the soil surface to be used to monitor landslide movements.

### 2.1. Basic principle of UWB

UWB is a radio technology that can use a very low energy level for short-range, high-bandwidth communications over a large portion of the radio spectrum (> 500 MHz); this should, under the right circumstances, be able to share spectrum with other users. In case of impulse-based UWB, one of the most appreciated application is the accurate ranging and high-precision localization capability (Win and Scholtz, 1998; Win et al., 2009). The idea is to send radio impulse from one module to another and measure the time of flight (ToF). Because radio impulses travel at the speed of light we can simply divide the ToF by this speed to get the distance. The wider the band of the signal, the smaller the impulse over time. This makes the estimation of the distance more accurate, since the reflections of the transmitted impulsive signal do not overlap at the receiver. The UWB signals that are used in our modules have a bandwidth of 500 MHz resulting in 0.16 ns-wide pulses. This timing resolution is so fine that at the receiver, we are able to distinguish several reflections of the signal. Hence, it remains possible to do accurate ranging even in places with many reflectors, such as in landslides.

An obstacle between transmitter and receiver, i.e., non-line-of-sight (NLOS), implies a bias in the estimation of the distance. For this reason, it is important to try to install all the sensors so that they are visible to each other.

In the Wi-GIM system, the UWB chipset is used for both localization (i.e., for measuring inter-node distances) and communication between nodes; therefore, there is no need to implement a sensor dedicated to measurements, with consequent savings in terms of cost and energy.

### 2.2. Hardware configuration and performance

A single node is basically an electronic board with several components and an intelligence which controls them.

The board is designed to host the microcontroller, while all the other components are external I/O. Each node can be then equipped with different components/modules. Depending on how such components/modules are combined, distinct types of nodes with different functions can be implemented. The standard components for master and slave nodes used for Wi-GIM are:

1. master node: this device includes the following modules: SD memory card, microcontroller ARM Cortex M3, battery, UWB module for communication and ranging, GPS, GSM/GPRS/3G communication module;
2. slave node: this device includes the following modules: microcontroller ARM Cortex M3, battery, UWB module for communication and ranging.

A single master node and a group of slave nodes (from 1 to typically 15) constitutes a cluster. Larger clusters are possible but would increase the number of transmissions (since every node communicates with each other visible node) thus reducing the battery life.

The communication module (GSM/GPRS/3G) is used to send remotely (on a web page) a periodical report on the status of the cluster/network with all the distances measured/collected by the master, and other useful information such as battery level, possible non-responding nodes, the temperature, etc.

The UWB hardware is the Decawave Sensor DWM1000 Module (2017a). It integrates antenna, all radiofrequency circuitry, power management and clock circuitry in one module (Fig. 1). It can be used in two-way ranging or ToF location systems to locate assets to a precision of 10 cm and supports data rates of up to 6.8 Mbps.

The antenna used in the module is the Abracon ACA-107-T dielectric chip antenna (3200–7200 MHz frequency range), part number ACS5200HFAUWB. See Abracon (2017) and Mouser (2017) for the data sheet and full details. The radiation patterns, measured in an anechoic chamber for three planes, are shown in Decawave (2017b).

The expected error of the distance measurement is 10 cm over 150 m. This is a nominal value, in ideal conditions: line-of-sight (LOS) and one-shot measure. This performance can be improved by applying digital processing techniques over several measurements, which can decrease the error down to 2–3 cm. This will be discussed in Section 2.4.

The operating range of the sensor nodes has been experimentally tested. Nodes can communicate and perform the ranging procedure properly up to 150 m in LOS condition, although Decawave data sheet reports 290 m. NLOS condition can decrease the accuracy of the ranging, as well as the quality of communication between nodes (Falsi et al., 2006). The precision in NLOS condition has been measured to be in the range 20–50 cm, depending on the nature of the obstacle (stone, tree, bush, etc.).

### 2.3. System architecture

The system architecture (Fig. 2) is master-slave: a master node coordinates the actions of the slaves under its control. In particular, it is an ad hoc network using a modified star topology. The master coordinates the slave sensors by determining which slave should be activated; then the slave measures the distance between itself and all the surrounding nodes (slaves and master alike), occupying the channel (as

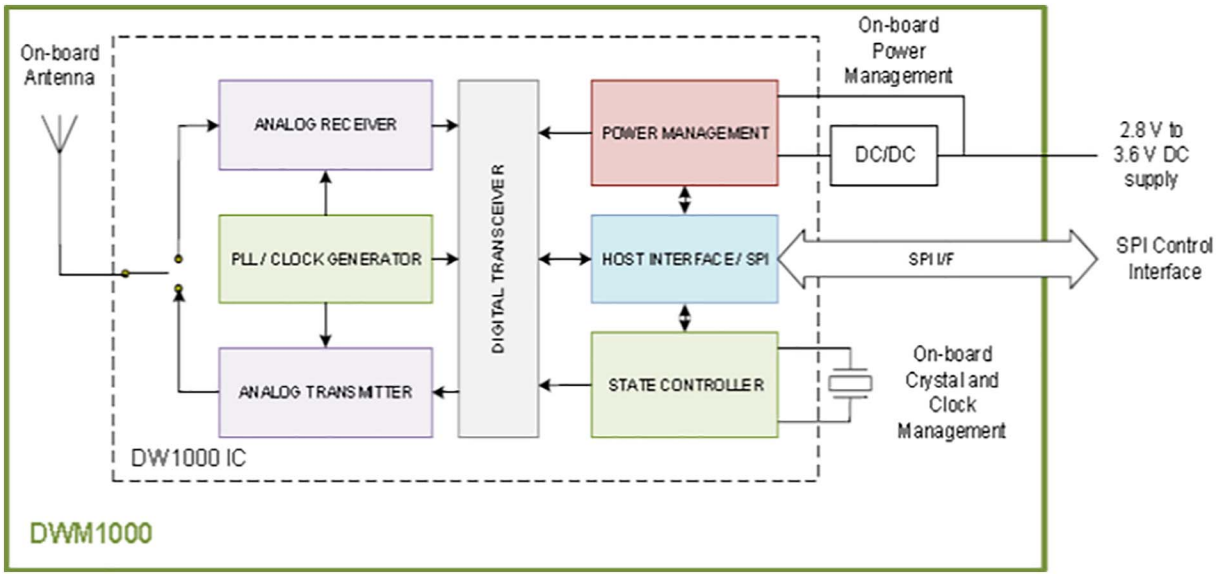


**Fig. 1.** Block diagram of Decawave UWB module.

described in Section 2.4). When the slave has completed the distance measurements, it sends the results to the master and then releases the channel. The master can now send the activation control signal to another slave. And so on, until all the slaves are activated.

The master might not see all the slaves directly. However, it has the information, coming from the initial network scanning, of which are the nodes that each slave is able to reach. This makes the master able to draw a sketch of the network connections between the nodes. Hence, a slave that is not directly seen by the master can anyway be activated by another slave, which can relay the commands of the master to the final destination node.

The definition of ad hoc refers to the possibility to relay the master commands to all the network nodes, and also to the fact that any node can be set as a master.

Each node is equipped with a microcontroller, a UWB module, a battery and a power supply (Fig. 3). The power supply is a 12 V, 7.2 Ah lead acid battery, but in the future a lithium rechargeable battery can be integrated into the UWB module. The master node also has a memory card and a GPS module. The GPS is not required for positioning but for a time reference. The master node spreads the GPS time reference among the slaves before starting the ranging measurements. During the ranging procedure, the master node commands each slave to measure the distance to the surrounding nodes that are visible to that node. The master has in memory the IDs of the slaves, as well as how many hops are required to reach each specific node. The distances measured by a node and the time stamp are sent to the master, which stores the information in its memory card. After all the distances are collected, the master sends the report file to the cloud server via 3G connection. The master also collects the battery level information from the slaves and put it into the report file.

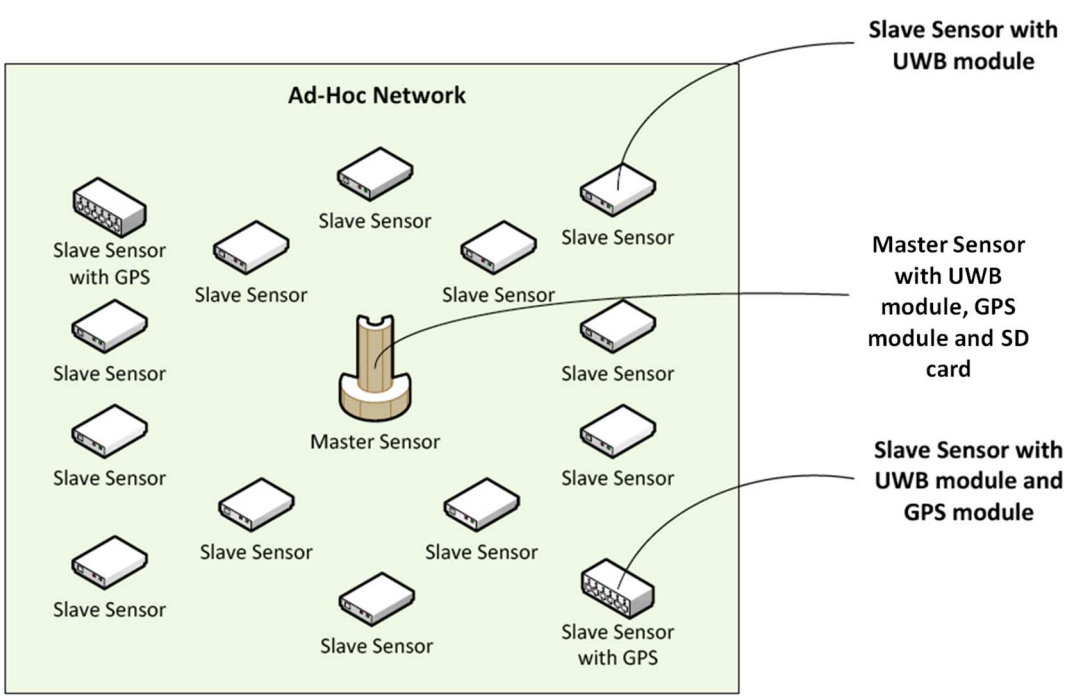


**Fig. 2.** Wi-GIM system architecture.

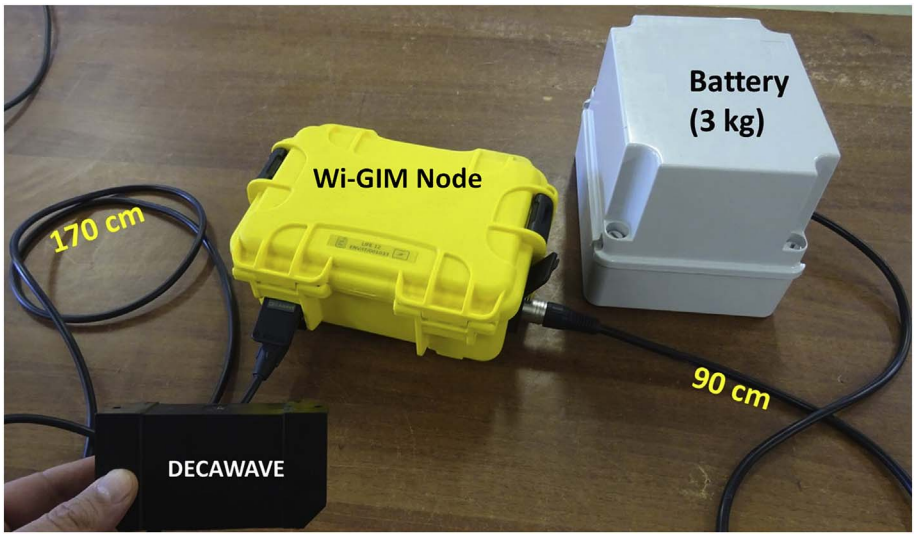


**Fig. 3.** Components of a Wi-GIM slave node.

Since battery consumption is a critical point for the WSN, a sleep mode is implemented for the nodes. The master node is programmed to periodically measure the distances throughout the day, e.g., every 10 min over 24 h. Once a complete scan of the nodes is finished, the master sends the sleep command and the wake-up time to the slaves. All the nodes deactivate all their power-consuming modules and then reactivate them at the programmed time. A single entire measurement cycle (from activation to back in sleep mode) lasts around 90 s. For an earth flow (like the one described in Section 4), given its slow temporal evolution, the measurement frequency can be 2–4 acquisition per day in order to save batteries. For a longer use of the WSN on a landslide, the battery of each node can be changed without moving the node.

### 2.4. Data analysis and processing

When a node is activated by the master, it sends an UWB impulsive signal to each near node with which it is able to communicate. The neighbor node receives it and sends it backwards. The active node thus can estimate the inter-node distance by calculating the two-way ToF. Once the ToF is estimated, the distance is obtained by multiplying the ToF times the speed of light. This computation is made by the master sensor.

The post-processing is carried out after the data are collected by the server, with the use of specifically created Matlab functions used for data filtering (see Section 3.1), for automatically comparing displacement velocities with fixed thresholds and sending automatic notifications, and also for plotting the displacement diagrams of all the possible combinations of nodes, useful for advanced analyses by the operators. Each master sensor sends the collected data (distances between its network nodes, temperature, battery levels, etc.) periodically by using the GSM/GPRS/3G module. The basic processing is: 1) the outliers identification and removal; 2) temperature-dependent error correction; 3) averaging over several measures (e.g., one day); 4) constant offset correction. The constant offset is an effect of multiple echoes at the receiver.

## 3. Field tests

### 3.1. Cluster installation

To perform field tests on the Wi-GIM technology, six clusters were installed in an open environment located in Arcetri, Florence (Central Italy). The test site was chosen for logistic reasons (namely, accessibility and therefore the possibility to easily change acquisition parameters and the setting and position of the nodes) and due to the site characteristics (e.g., an outdoor setting with heterogeneous vegetation), which allowed us to test the effects of obstacles and temperature on the measurements. No landslides or ground movements were expected in this site, but the nodes were moved manually, if needed. This allowed us to determine the precision of the system and the factors of influence, being sure that real movements should have been excluded.

For each specific test, a different cluster was installed, with an acquisition frequency of 1 measurement per 10 min, taking advantage of the site characteristics and the available distances (Fig. 4). A cluster is defined as a group of slave sensors (up to 15) managed by a single master sensor. In particular, it is defined by a single master when the scanning procedure starts during the configuration of the sensor network. During the scanning procedure, the master sensor uses the communication control channel sending a request signal. Slave sensors around the master answers to this signal with an ACK (acknowledge) and the estimated distance. Once the master has collected all of the ACKs, it defines its network (cluster) of sensors, which are managed by itself from that time on. After this procedure, the master sensor has in memory the “web” (the lines/distances between nodes) of the slave sensors within its network.

Data were processed through the following steps implemented in Matlab:

- distances measured by the master node were plotted as a function of time (raw data, Fig. 5A);
- values equal to zero and non-numerical values were removed (valid data, Fig. 5B);
- outliers were identified and removed, with outliers considered values with a distance > 1 m compared to the previous value, including multipath effects (corrected data Fig. 5C);
- since a correlation with the temperature was identified (see following section), the effects of temperature on the measurements were filtered (filtered data, Fig. 5D).

A further improvement can be achieved by taking advantage of the system redundancy. In fact, the distance between two nodes is measured by each node (e.g. node x measures its distance from node y and then node y makes the same). This results in double measurements for each distance, so an acquisition frequency of 4 measurements per hour actually produces 8 values. Therefore, the simple average between these measurements gives a better approximation of the real distance and contributes to further increase the precision.

During the field test in Arcetri, the standard deviation of raw data

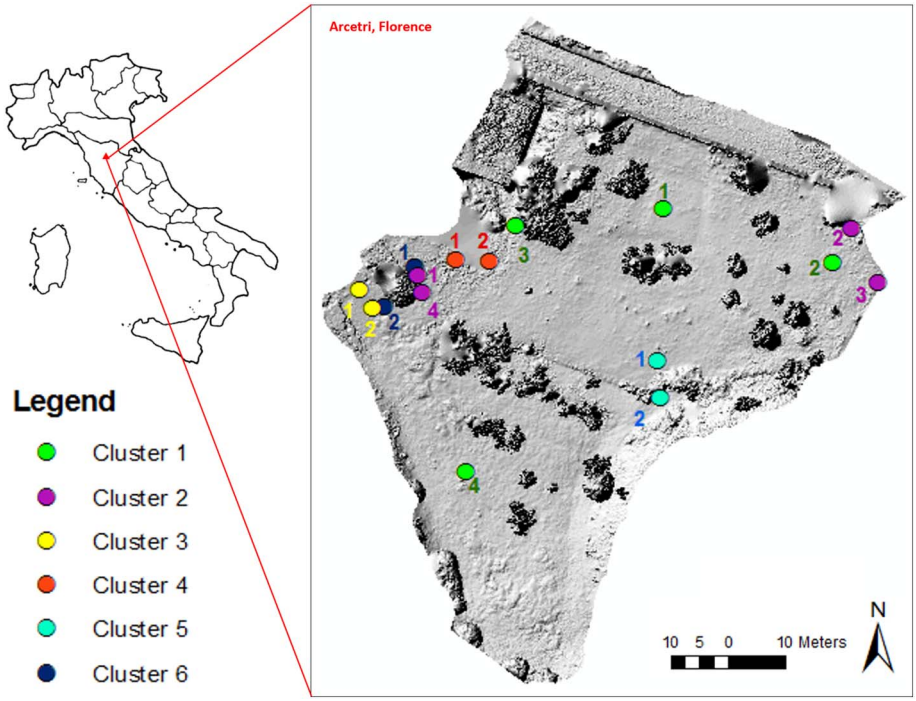


**Fig. 4.** Location of the experimental field test in Arcetri. The nodes indicated with the number "1" are the masters for the respective cluster.

has been calculated as 1.37 m (on average among all the clusters), which was largely affected by outliers and zeroes. After the application of the filtering above-mentioned procedure (comprising the temperature filtering explained in the next paragraph), the standard deviation was 0.015. If data are further averaged in order to obtain a daily mean a standard deviation of 0.013 can be attained.

### 3.2. Temperature influence

Air temperature measurements are performed at every measuring cycle using a sensor placed on every master node. This value showed a strong correlation between the measured distances and temperature on a daily scale (Fig. 5C). The data analysis highlighted a linear correlation between these parameters described by a trend line (Fig. 6, Table 1).

For this reason, we propose a linear model of the relation between ranging and environmental temperature. The proposed relation is therefore "empirical", since, it is based on -field observations.

A correction taking into account a standard temperature of 20 °C was made using a correction factor $K_i$ for each displacement value:

$$K_i = (\mathrm{T_i} - 20) * m$$

where $m$ is the trend line slope (angular coefficient) and is constant in time for each couple of nodes but it varies from couple to couple; $\mathrm{T_i}$ is the temperature measured at the time ($t_i$) of the acquisition that is going to be corrected.

The correction was applied by subtracting $K_i$ from each value, resulting in a consistent reduction of the data variance:

$$D_i = D_0 - K_i$$

where $D_0$ is the raw measured distance (that is the output value before the temperature correction) and $D_i$ the corrected value of the distance. The satisfactory results of this correction are clearly visible in Fig. 5D, which shows how data are no more following the temperature oscillations.

Furthermore, to verify whether this relation depended on distance, data from Cluster 2 were also analyzed since its nodes provide the possibility to examine both long and short distances (Table 1). It was not possible to analyze nodes 2–4, the most distant from each other, because their inter-visibility was compromised by vegetation.

It appears that the values of the angular coefficient are similar between different couples within the same cluster (regardless of their respective distance) while they vary from a cluster to another. Therefore, other factors than the inter-nodes distance probably influence the relationship between temperature and ranging measurement. For example, it is possible that $m$ is also affected by the internal temperature of the nodes or by local atmospheric effects (such as variation of humidity or turbulence), especially where the LOS is close to the ground. This means that, for a proper filtering of temperature effects, the value of $m$ cannot be assumed but needs to be calibrated for each couple in every application.

In order to apply the temperature correction, a preliminary period of acquisitions is necessary to calibrate the relationship between temperature and distance. Once that $m$ is calculated for each couple of nodes, it can be used to correct the value of $D_0$ after calculating $K_i$. This correction is real-time and therefore does not invalidate early warning applications.

### 3.3. Inter-visibility tests

An initial inter-visibility test was performed by tying the antennas to stakes approximately 25 cm high so that the antennas were only a few centimeters above ground level. However, in this configuration, the nodes were not able to properly communicate, probably due to the presence of abundant grass cover combined with small slopes and ground bumps. Therefore, the clusters were reinstalled at the same positions but on stakes 1-meter high. This change enabled reciprocal visibility between all nodes.

Subsequently, a series of tests were conducted to study the system behavior in case of obstacles; for this purpose, clusters composed by one master and one slave node were used.

First, to determine how an obstacle could influence the measurements, a 40-cm wide and 2 m high hollow plastic cylinder was installed between two nodes (Cluster 3) spaced 3.30 m apart (Fig. 7A).

After 8 days of acquisition, the obstacle was removed. The results showed that the obstacle influenced the ranging measurements (Fig. 8A). In particular, while the data dispersion (and therefore

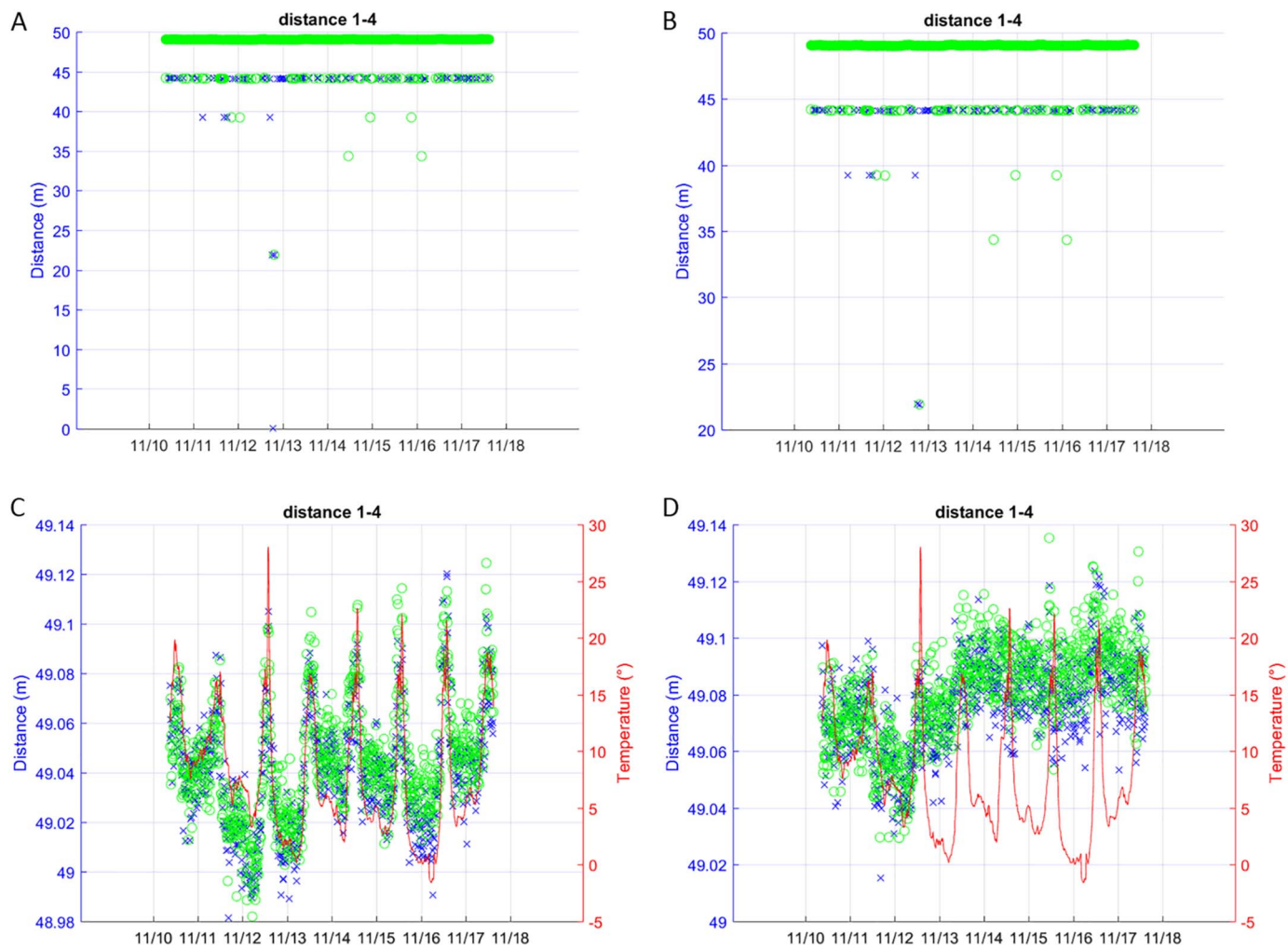


**Fig. 5.** Example of the data filtering steps executed on nodes 1–4 (Cluster 1) in November 2016. Green circles and blue crosses represent the distance measured from one node to the other and vice versa. Where measurement points are extremely dense, the blue crosses are overlaid by the green circles. (For interpretation of the references to colour in this figure legend, the reader is referred to the web version of this article.)

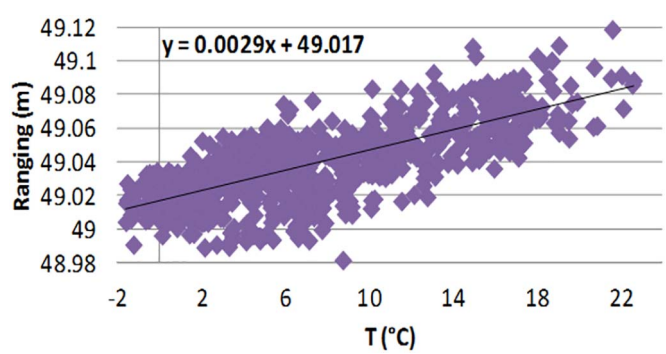


**Fig. 6.** Scatter plot between the temperature and the measured ranging, calculated for the couple of nodes 1–4 belonging to Cluster 1.

precision) was not affected by the obstacle, a shift of a few centimeters between measurements before and after object removal was observed, affecting the measurement trueness. Specifically, in the first days of acquisition (when the obstacle was in place), longer and less reliable distances were measured by the monitoring system. This phenomenon was interpreted as related to a difference in the path travelled by the waves that, with a completely solid obstacle obstructing the LOS, were still able to reach the antennas but only after one or more rebounds.

Notably, even without obstacles, the ranging distance measured by Wi-GIM is still affected by systematic error resulting in an offset with respect to the actual distance. This value is constant for a specific pair of nodes but varies from pair to pair. It is probably due to a partial calibration of the circuits at the factory level caused by a wrong estimation of the time needed for the signal to cover the distance between its generation and its amplification. However, it is important to highlight that the determination of absolute distance is not relevant for the applications of Wi-GIM; since it is designed for displacement monitoring and early warning, only the variation of distance is important.

**Table 1**
Distances and trend line slopes of pairs of nodes for clusters 1 and 2 at Arcetri.

| | Nodes | Distance (m) | Angular coefficient | Coefficient of determination $R^2$ |
|---|---|---|---|---|
| Cluster 1 | 1–4 | 49 | 0.0029 | 0.5340 |
| | 3–4 | 38 | 0.0025 | 0.3091 |
| | 1–3 | 22 | 0.0030 | 0.4803 |
| Cluster 2 | 1–4 | 3 | 0.0070 | 0.7394 |
| | 3–4 | 67 | 0.0060 | 0.7063 |
| | 1–3 | 67 | 0.0063 | 0.8151 |

The same hypothesis is consistent with the other tests.

Another experiment involved flipping the antennas of Cluster 1 of 180° on their vertical axis to see whether the measurements were affected. This test was important because it was necessary to prove that a


**Fig. 7.** Photographs of different configurations for the inter-visibility tests with a PVC pipe (A), a tree (B), a vegetated bush (C) and a dry bush (D).

node could effectively make measurements, even with respect to other nodes behind it, in a common configuration in a fully connected monitoring network. This experiment resulted in a shift in ranging measurements of all the couples of nodes (from 5 cm of nodes 2–4 to 20 cm of nodes 1–2, with the average being around 10 cm), which could be explained by the different wave paths that rebounded several times on obstacles before arriving at the receiving antenna. Since the boundary conditions were different for each node, the shift value changes from node to node.

Further tests were performed to evaluate the system behavior with different types of obstacles, such as a 40-cm wide tree trunk (Cluster 4). The antennas were initially positioned at the sides of the trunk, each at a distance of 1.20 m. After a week, the antennas were moved an additional 1 m from the obstacle for a total distance between them of 4.40 m. They were then moved again and reinstalled 5 m from the trunk, for a total distance of 10.40 m (Fig. 7B). The data showed the signal was able to transmit despite the presence of the trunk (Fig. 8B). The same results were observed for each evaluated distance, without an evident relation between the obstacle influence and its distance from the nodes.

The effect of different vegetation types was then analyzed taking into account a densely vegetated 7 m tall, 4 m wide shrub (monitored by Cluster 6) and a 1.5 m tall dry bush (monitored by Cluster 5). In both cases, the antennas were positioned at opposite sides of the obstacle at 7.50 m (Fig. 7C) and at 5.34 m (Fig. 7D) and the signal was able to bypass the obstacle despite the antennas being close to the obstacle (Fig. 8C, D). Notably, the test conducted using Cluster 5 showed a sensible ranging shift starting from February 1st, indicating an increased distance between nodes, which can be interpreted as a variation in the geometry of the branches within the shrub.

The comparisons between the real distances between the nodes (measured with a laser distance meter) and the distances measured with Wi-GIM are reported in Table 2. Note that, for every case, the LOS was never completely free of obstacles, although their nature and dimension varied from case to case. The couple 2–4 of Cluster 2 is not included since not visible by Wi-GIM.

## 4. Roncovetro landslide application

Experimentation on an actual case of instability was performed to stress test the system.

The chosen site was the Roncovetro landslide, a 2.5 km long complex landslide with a volume of 3 million $m^3$, first described by Almagià (1907). It is located in the Emilia Romagna Region (Northern Italy) and carves the southern slope of Mount Staffola (where the crown is located) down to the Tassobbio Stream (at the toe), where it partially dams the watercourse, creating a small seasonal lake (Fig. 9).

The landslide material is formed by shaly-clayey calcareous-arenaceous flysch (Mount Staffola Formation, Cretaceous-Eocene), whose original well-layered structure has been almost completely lost, due to tectonic stresses acting during the Apennine orogenesis. As a consequence, the clay fraction is dominant in the landslide, as a “matrix” that includes rock blocks of various size and lithology. This causes the landslide to behave as a fluid-viscous mudflow, with maximum velocities up to 10 m/day, except for the head, which behaves as a translational earth-slide (Bertolini, 2010; Bertolini and Fioroni, 2013). The landslide alternates seasonal phases of suspension (as defined by Cruden and Varnes, 1996) with phases of activity and, sometimes, paroxysms. Archival documents cite the landslide reactivations occurring 10 times in a 100-years period (Bertolini, 2010). This very peculiar behavior is favored by the inflow of mineralized ground-waters, mixed with methane, coming from the subsurface.

A distinctive feature is the long and narrow channel, 30 to 40 m wide, deeply carved into the flysch bedrock, which links the depletion zone to the accumulation zone. During the last 20 years, the average speed of the mudflow has been of 33.6 m/year. The maximum observed velocity, in the upper part of the landslide, was 9 m/day (Bertolini, 2010; Bertolini and Fioroni, 2013).

The upper and central parts of the Roncovetro landslide were considered optimal for the Wi-GIM experiment due to several factors:

1) the landslide shows almost continuous movement;
2) as a consequence of the different mechanisms of rupture (deep creep, sliding, flowing), the upper area of the landslide shows a very large range of displacements;
3) the possibility to cover the whole width of the landslide in the central part;
4) a variety of field conditions enabling the inter-visibility of the monitoring network nodes and also investigation of the effect of obstacles;

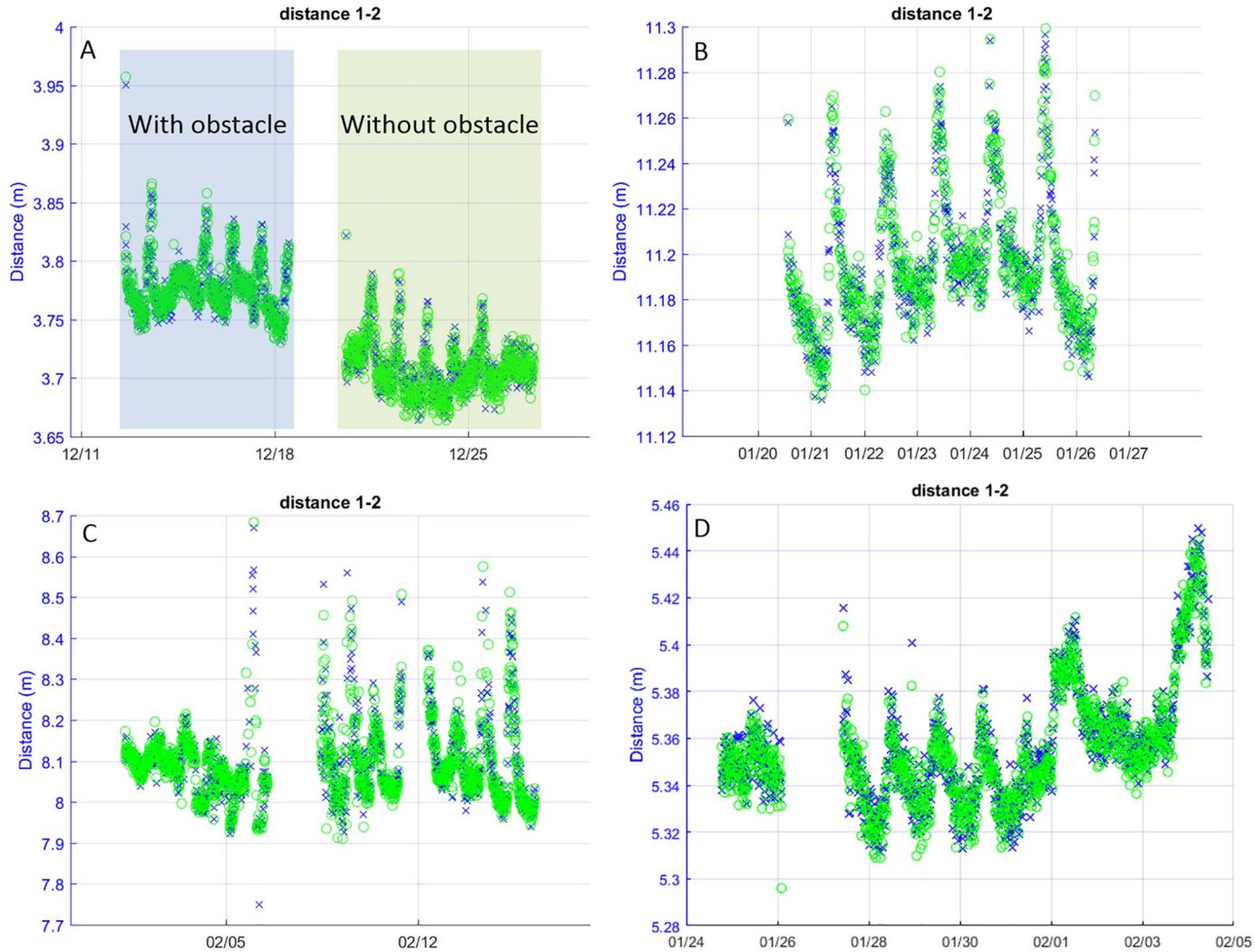


**Fig. 8.** Measurements of the distances between nodes with time. Each graph (A, B, C, D) corresponds to the respective experiment shown in Fig. 7A, 5B, C, D. Periods of non-acquisition were due to a lack of power. Green circles and blue crosses represent the distance measured from one node to the other and vice versa. Where measurement points are extremely dense, the blue crosses are overlaid by the green circles. (For interpretation of the references to colour in this figure legend, the reader is referred to the web version of this article.)

**Table 2**
For each couple of each cluster is reported the real distance between the nodes (measured with a laser distance meter), the minimum, mean and maximum distance measured with Wi-GIM, the standard deviation σ of Wi-GIM measurements and the difference between the real distance and the mean measured by Wi-GIM.

| | Nodes | Real distance (m) | Wi-GIM distance (m) | | | σ (cm) | Difference (m) |
|---|---|---|---|---|---|---|---|
| | | | Min. | Mean | Max. | | |
| Cluster 1 | 1–2 | 25.62 | 25.08 | 25.16 | 25.23 | 2.5 | 0.46 |
| | 1–3 | 21.35 | 22.65 | 22.90 | 23.15 | 2.2 | 1.55 |
| | 1–4 | 48.16 | 49.03 | 49.08 | 49.13 | 2.1 | 0.92 |
| | 2–3 | 45.87 | 45.64 | 45.70 | 45.76 | 2.1 | 0.17 |
| | 2–4 | 61.10 | 62.14 | 62.23 | 62.27 | 1.7 | 1.13 |
| | 3–4 | 37.08 | 37.70 | 37.75 | 37.80 | 2.2 | 0.67 |
| Cluster 2 | 1–2 | 65.50 | 64.16 | 64.21 | 64.25 | 1.3 | 1.29 |
| | 1–3 | 66.70 | 67.28 | 67.30 | 67.40 | 2.3 | 0.6 |
| | 1–4 | 2.56 | 2.80 | 2.85 | 2.90 | 3.0 | 0.29 |
| | 2–3 | 8.47 | 8.70 | 8.80 | 9.10 | 2.8 | 0.33 |
| | 3–4 | 66.36 | 66.98 | 67.02 | 67.07 | 2.8 | 0.66 |
| Cluster 3 | 1–2 | 3.30 | 3.74 | 3.76 | 3.85 | 3.0 | 0.46 |
| Cluster 4 | 1–2 | 10.40 | 11.13 | 11.20 | 11.28 | 2.6 | 0.80 |
| Cluster 5 | 1–2 | 5.34 | 5.30 | 5.35 | 5.42 | 3.7 | 0.01 |
| Cluster 6 | 1–2 | 7.50 | 8.00 | 8.20 | 8.60 | 5.0 | 0.70 |

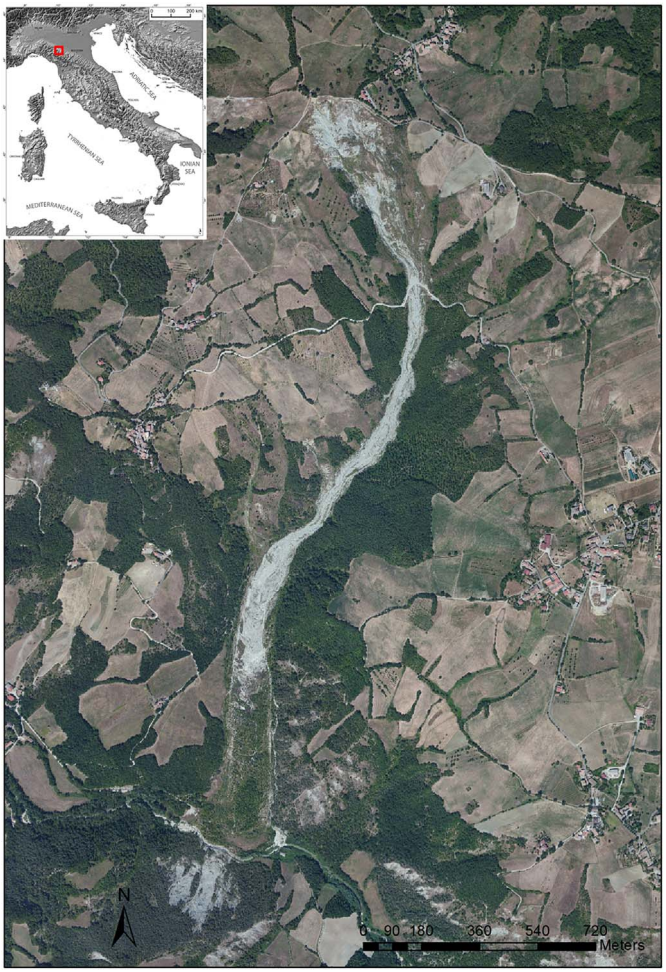


**Fig. 9.** Aerial photograph of the Roncovetro landslide.

5) sufficient size to test the range limit of the network;
6) the possibility to implement a parallel system of monitoring (automated geodesy) by using a robotic total station to cross-check and validate the Wi-GIM data.

Therefore, two clusters were installed, one on the fastest moving sector of the depletion zone (Cluster 2) and one on the narrowest part of the mudflow (Cluster 1), as shown in Fig. 10A. Measurement validation was performed using an RTS by installing prism targets and Decawave antennas on the same poles (Fig. 10B, C). Cluster 1 was composed of 11 nodes, with 3 placed outside the landslide as reference points on stable locations (number 1, 2 and 7). Cluster 2 was composed of 12 nodes, with the master node installed at the center of the network; in this cluster, to stress-test the system, the nodes were placed at longer internode distances (up to 190 m from one end of the cluster to the other, which, as expected, turned out to be above the maximum distance required for granting a good communication) so that the entire crown area was covered. Furthermore, this second cluster was purposely tested without using any reference point; in fact, since the landslide experiences differential movements, the presence of an external reference is not necessary for our aims and early warning purposes.

The acquisition frequency was calibrated based on the velocity of the mudflow and set to record 1 reading every 6 h. The measurements are redundant (as they are performed from one node to another and vice versa), which makes it possible to calculate the daily averaged using a total of 8 readings to reduce noise.

The RTS was a LEICA NOVA MS50 3D Multistation installed in a stable area near Cluster 1 in a location where all nodes were visible (Fig. 10A).

The comparison between the Wi-GIM and RTS measurements shows an offset relative to the measurement of the absolute distance (Fig. 11A) due to the effects described in Section 3.3. Although this offset is not relevant for monitoring dedicated to distance variation (which is the only parameter that matters for early warning purposes), since it is constant for a given pair of nodes, it was corrected (Fig. 11B). The result highlighted a strong correlation between measurements.

Between May and June 2016 the Wi-GIM nodes recorded an acceleration, while RTS did not generate any recording because the pole slowly tilted and finally fell down. Whereas the RTS lost sight of the prism mounted on the pole and was not able to perform further measurements, the Wi-GIM nodes continued to detect displacement. July 2016 records an abrupt increase of the distance (around 1 m) due to the correct repositioning of the pole.

The long monitoring time enabled observations of the effect of the seasonal variation of temperature on the data. This variation caused an artifact of +10 cm in the total accumulated displacement from winter to summer. For the daily oscillations, a similar procedure reduced the influence of long-term temperature effects. On the other hand, no disturbance due to rain or snow was observed, both in terms of precision and data transmission.

The Roncovetro experiment was also able to assess the effects of long distances on the overall performance of the system. While distances longer than 100 m resulted in more difficult transmission, they did not affect the measurement precision or trueness. More specifically, the distance between nodes was studied in relation to the precision of the measurements by calculating the standard deviation (σ) of measurements made at different distances. Pairs 3–4, 1–3 and 1–7 for Cluster 1 and pairs 2–11, 1–2 and 5–12 for Cluster 2 were examined. To evaluate the data dispersion, the data were analyzed during periods of stability for each pair (from 11 March 2016 to 31 May 2016 for Cluster 1 and from 1 December 2016 to 6 February 2017 for Cluster 2), to ensure that the measurements were not related to actual movement. All selected pairs were characterized as a percentage of received data > 80% and a percentage of valid data > 60%. The results of this analysis did not indicate a correlation between distance and Wi-GIM precision (Table 3).

Similarly, a study was conducted to investigate the effects of rain and snow effects on Roncovetro's clusters; here, we were not much interested in seeing how rain and snow affected the landslide, but how they affected the monitoring system. For rainfall, rain gauge data from a meteorological station previously installed in the area were used. For snow, only information about the occurrence of snowy days was available. Fig. 12 shows an example of the analysis for pair 4–9 of Cluster 1, highlighting a basically stable situation and how rainfall and snowy days are not associated with spikes or increased noise.

When a node is visible to at least 3 other nodes, the Wi-GIM system can determine its planimetric position and track its variation with time; in fact, the intersection of three circles individuates an elliptic triangle whose center has been taken as the position of the node. This motion tracking feature was tested and compared with the results from the geodetic monitoring (Fig. 13). In Fig. 13A, both systems tracked a movement of approximately 3.8 m toward SE from February to September 2016. Although with a higher data dispersion, Wi-GIM correctly traced the direction and module of the displacement vector. Fig. 13B to Fig. 13E show the same type of datum but for Cluster 1, where the movements were lower. In fact, even though data dispersion here seems to be higher than that in Fig. 13A, this is only because the scale is magnified 10 times. This enables to assess that the localization precision is of the order of ± 5 cm for every node, which can be easily improved using a mean of data. The directions of movement are also in good agreement with the RTS prisms and with the geomorphology of the landslide, indicating a movement toward SE, SSE or S, that is visible as soon as the total displacement is higher than the precision of the system. Fig. 13F shows node 5 from cluster 1 during a 2-months period

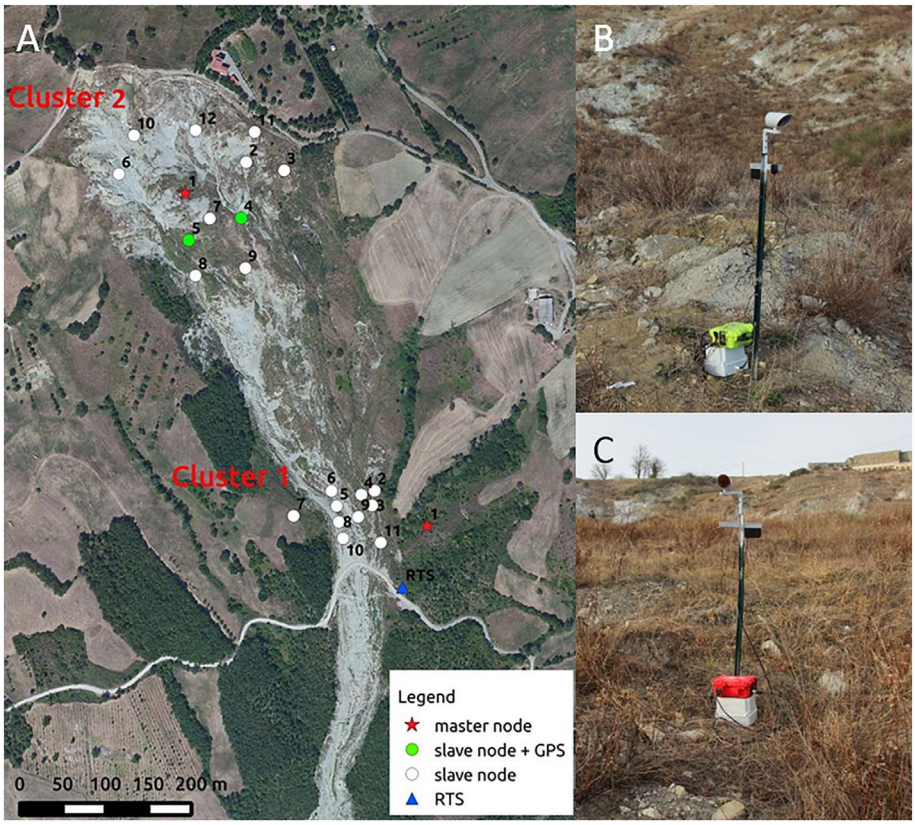


**Fig. 10.** A: location of the Wi-GIM nodes and the RTS installed at Roncovetro; nodes 1, 2 and 7 are places outside the landslide in a stable location. B, C: Wi-GIM nodes and RTS prisms.

of stability. The average distance of each measurement from the center of the cloud has been calculated to obtain an estimation of the precision for a stable node; for the RTS we obtained 0.44 cm and for Wi-GIM 3.44 cm.

## 5. Discussions

In order to quantitatively evaluate the Wi-GIM performance and its variation over time, a specific index, called Performance Index (PI), has been introduced. The analysis of the PI values plotted vs time allowed us to assess possible local anomalies, making it possible to change the system settings in progress, to achieve the best results in terms of data quality and continuity.

PI is calculated daily for each couple of nodes, and is defined as the product of two parameters:

$$PI = P1 \times P2$$

Each parameter is defined as follows:

$$P1 = N_v/N_{tot}$$

$$P2 = 1 - D$$

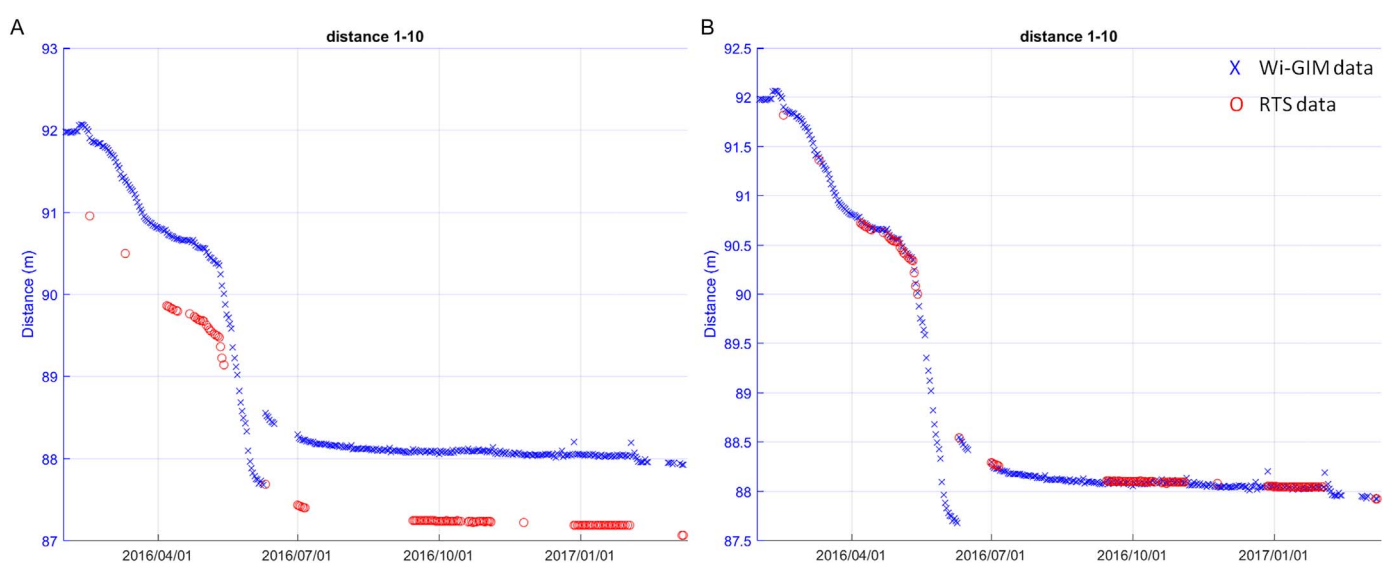


**Fig. 11.** Displacement time series of the pair of nodes 1–10 of Cluster 2 from February 2016 to March 2017. Blue crosses: daily averages of filtered Wi-GIM data. Red circles: RTS data. A: data without offset compensation. B: compensated data. (For interpretation of the references to colour in this figure legend, the reader is referred to the web version of this article.)

**Table 3**
For each couple of each cluster is reported the real distance between the nodes (measured with RTS), the mean distance measured with Wi-GIM, the standard deviation σ of Wi-GIM measurements and the difference between the real distance and the mean measured by Wi-GIM.

| | Nodes | Real distance (m) | Wi-GIM mean distance (m) | σ (cm) | Difference (m) |
|---|---|---|---|---|---|
| Cluster 1 | 3–4 | 14.49 | 15.09 | 4.7 | 0.60 |
| | 1–3 | 69.18 | 69.88 | 3.5 | 0.70 |
| | 1–7 | 131.90 | 132.75 | 2.6 | 0.85 |
| Cluster 2 | 2–11 | 36.70 | 37.35 | 3.6 | 0.65 |
| | 1–2 | 80.13 | 80.83 | 3.0 | 0.70 |
| | 5–12 | 129.21 | 130.61 | 3.4 | 1.40 |

where $N_v$ is the number of valid distance readings (outliers and invalid measurements excluded) for each couple of nodes; $N_{tot}$ is the total numbers of readings requested by the master node; $D$ is the difference (expressed in m) between the RTS distance and the Wi-GIM distance (with the offset compensated). Therefore, PI takes into account the efficiency of data communication (indexed by P1) and the trueness of the measurements (P2).

Since each parameters P1 and P2 vary from 0 to 1, PI ranges from 0 (minimum performance) to 1 (maximum performance). Thus, the index expresses the quality of each link over time by considering the communication capability of each couple of nodes and the correctness of the performed readings.

The introduction of PI allowed us to continuously evaluate the performance of each component of Wi-GIM system, as well as to make some local interventions to maximize the quality of monitoring data.

The values of PI calculated for each couple of nodes at the end of the monitoring period in Roncovetro have been represented on a map (Fig. 14).

As a general rule, we can notice highest PI values where the distances are lower, but there can be particular unfavourable positions that make a node less visible under certain points of view (see for example node 10 with respect to nodes 4, 3, 9, which are near but more or less aligned along a not clear cone of sight). P1 is the parameter which mainly affects PI and is mostly influenced by environmental disturbances (such as vegetation growth or bad weather conditions) that make the communication more unstable.

A possible application of Wi-GIM is rapid characterization or early warning in emergency conditions. Therefore, the portability and short time required for node installation are pivotal. The system offers the possibility to send warnings (e-mail, SMS) if fixed displacement thresholds are exceeded or if the battery needs to be charged.

GB-InSAR and RTS are two instruments that have early warning capabilities and can easily monitor large areas with a relatively small installation effort. For such reason, they can be considered the benchmarks with which Wi-GIM can be compared for a cost-benefit analysis (Table 4).

For the cost calculation, two different cases have been considered:

- Case 1: monitored area of 500 $m^2$;
- Case 2: monitored of 100,000 $m^2$.

When comparing the number of Wi-GIM nodes with the number of RTS prisms, some considerations are necessary; in fact, to be able to furnish the complete displacement vector like a prism, a node needs to be connected by at least other 4 nodes. If the network is properly installed, this is the case for every node. However, it is possible that some peripherical nodes may not have a connection with other 4, although they can still provide inter-distances with one to three of them and therefore be trackable in 2 dimensions. So, of the total number of nodes, it is safe to assume that few of them may not be able to provide 3 movement vector components. On the other hand, of the total number of RTS prisms, 1 or 2 of them are not meaningful for landslide movement monitoring as they are typically located on stable areas to calibrate the atmospheric contribution. Therefore, it is not possible to assess a precise proportion between nodes and prisms, since they are dependent on the way they are installed and the quality of data transmission; furthermore, we just considered the case when Wi-GIM can provide 3D vectors only to better relate them with the performances of RTS prisms, although, for practical purposes, planimetric vectors may be sufficient (as for the applications shown in this paper). After these considerations, in Table 4, we have assumed the optimal installation of a Wi-GIM network where all nodes are fully connected and have not considered the RTS prisms for atmospheric noise removal.

Note that the direct costs indicated for the RTS and GB-InSAR are relative to the renting cost of the systems for 1 year, since the purchase of the instrumentations would have been too high (several tens of thousands €) and so not comparable with Wi-GIM.

The column relative to the completeness of information concerns

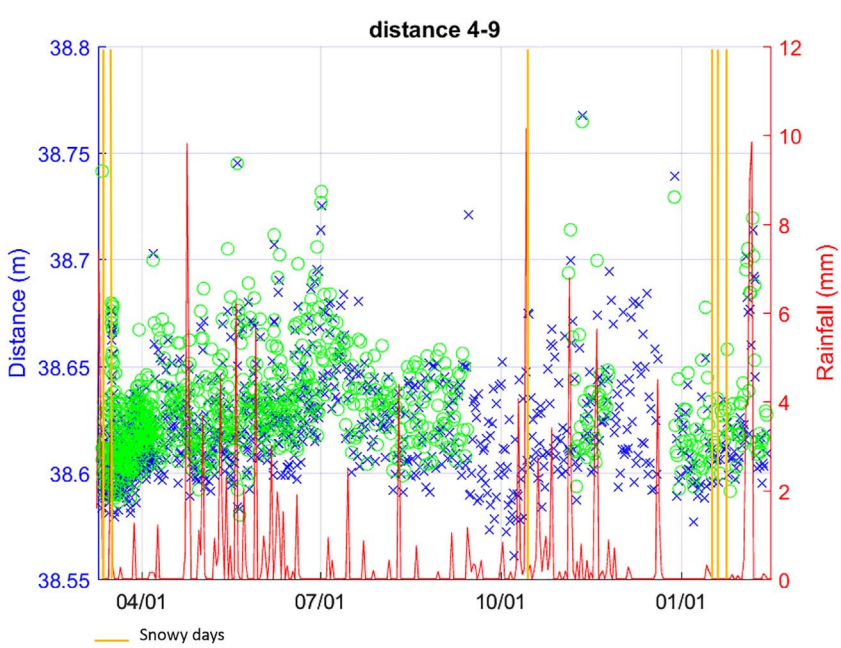


**Fig. 12.** Displacement time series of pair 4–9 of Cluster 1. Green circles and blue crosses represent the distance measured from one node to the other and vice versa. Where measurement points are extremely dense, the blue crosses are overlaid by the green circles. Daily rainfall is represented in red, while snowy days are in yellow. (For interpretation of the references to colour in this figure legend, the reader is referred to the web version of this article.)

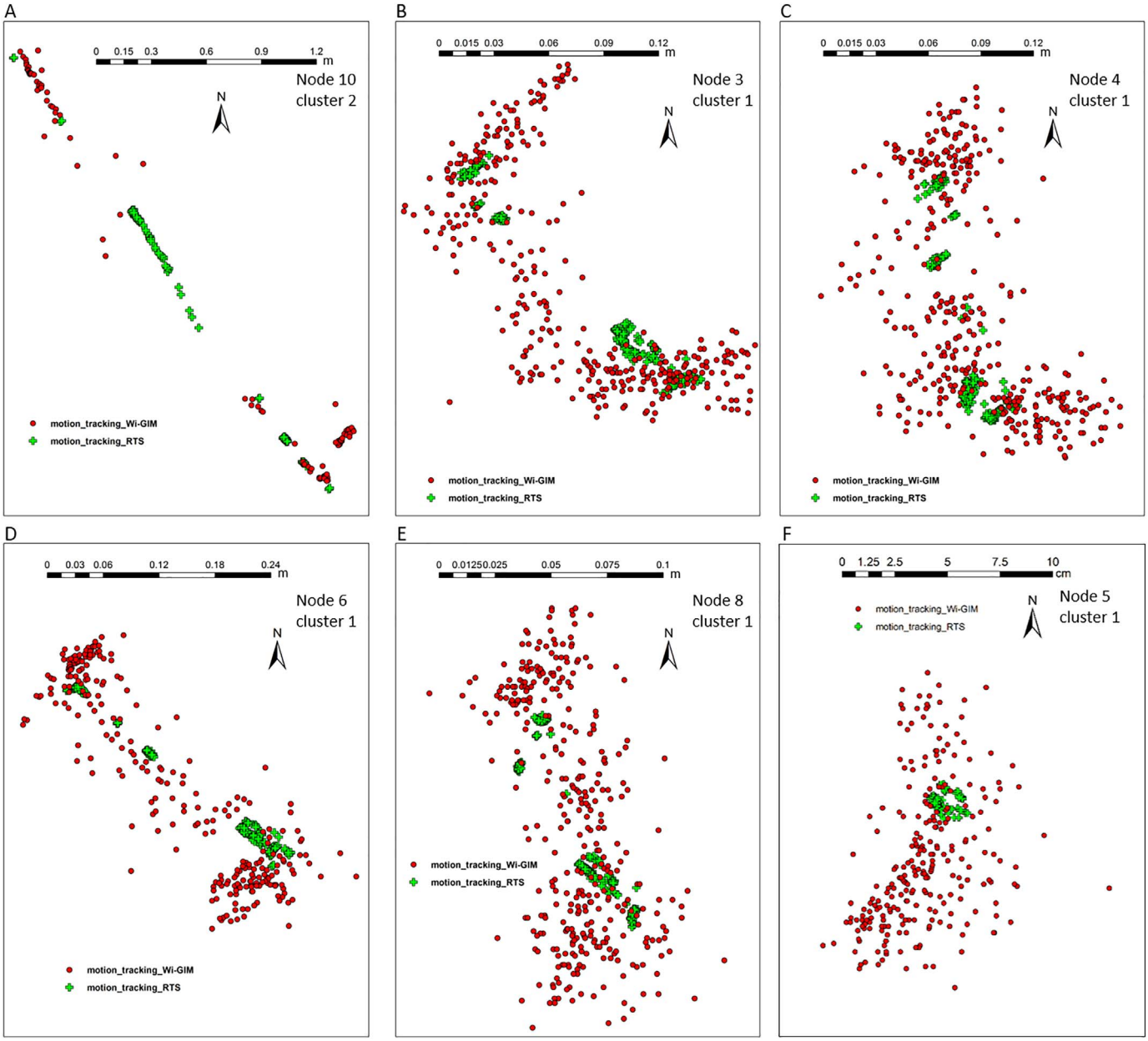


**Fig. 13.** Motion tracking of some nodes from Clusters 1 and 2 from February 2016 to September 2016. The crosses are RTS measurements; the circles are Wi-GIM measurements. Note that the scale of F is expressed in cm.

how many components of the movement vector are detectable for each instrumentation. GB-InSAR can only provide LOS measurements (1 component), RTS exploits 3D measurements and Wi-GIM lies in-between, as it performs from 1D to, potentially, 3D measurements depending on how many nodes are visible for a certain node.

Concerning the benefits, they have been evaluated according to the following scoring system:

- 1: poor;
- 2: fair;
- 3: good;
- 4: very good;
- 5: excellent.

Only assessing the benefits, the result in a lower performance of Wi-GIM with respect to RTS and GB-InSAR, especially due to the lower durability, precision and maximum range. However, considering the benefits in relation with the costs, Wi-GIM costs around 5 and 10 times lower than 1-year rental of RTS and GB-InSAR, respectively, concerning a monitored area of 500 $m^2$. This gap decreases as the area to be monitored increases, due to the cost of the single nodes, which is higher than the reflectors (for the GB-InSAR it is considered that no reflectors are needed).

The major limitation of the system is its comparatively low precision (2–5 cm on filtered data), which narrows its range of application to phenomena that undergo such movements during the monitoring time. Furthermore, it performs better (and costs less) on areas where long distances are not involved. However, Wi-GIM is still a prototype system, and features such as precision, cost, battery life, and node dimensions could be further improved with industrialization. Furthermore, since the system architecture is adaptable, it can be enhanced as technology advances and new low-cost hardware enters the market.

The system is versatile and modular and can be adapted to a large variety of scenarios with a low environmental impact. The acquisition

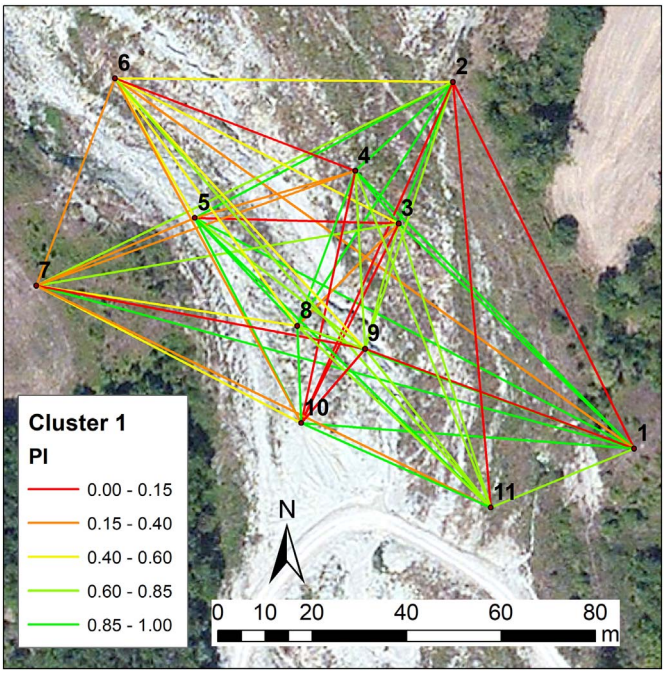


**Fig. 14.** Values of PI for each couple of Cluster 1 in Roncovetro.

frequency is a trade-off with battery duration and can be as high as 1 measurement every minute (or less if necessary). During the Roncovetro experiment, with a 2-hour acquisition interval, the battery life was approximately 35 days. Nodes can be easily added or removed if damaged or if greater network extension or density is needed.

Another interesting future application could be the monitoring of fractures and tension cracks. If two nodes are installed on the two sides of a fracture, they can simulate a wireless extensometer and measure the opening of the crack without the vulnerability and hindrance represented by a wire. Naturally, given the present precision of the system, this application would be usable for large rock slides experiencing displacements of the order of the meters.

## 6. Conclusions

In the framework of the European Life+ financing program for the environment, a new prototypical ground instability monitoring instrument, called Wi-GIM, has been developed. It consists of a WSN composed of nodes that can measure their mutual inter-distances by measuring the ToF of an UWB impulse. Therefore, no sensors are included in the network because the signals used for transmission are also used for ranging.

In the field of ground stability, encompassing both landslides and subsidence, there is a general lack of low-cost instrumentation to monitor displacement over a broad area. The main reason is the difficulty in providing good performance, especially in terms of precision, acquisition frequency and robustness. Although Wi-GIM is still a prototype system and, as such, is prone to improvements, it shows potential as an instrument for monitoring velocities classified as slow (on the order of 1 to 100 m/year) to rapid (m/min) (Cruden and Varnes, 1996), which are typical of earth flows, mudflows, subsidence in mining areas, earth slides, and rockslides after failure.

The system has been firstly implemented in a field test and then to monitor the displacement of an actual landslide, the Roncovetro mudflow in Central Italy. Data retrieved from the tests revealed that, besides outliers and multipath effect that were filtered with standard data processing, the measurements were influenced by temperature. After studying the correlation with temperature, a simple correction was sufficient to improve the precision and remove the effect of temperature.

The performed parallel monitoring using an RTS to validate the Wi-GIM results showed the presence of a constant offset due to miscalibration of the UWB modules. This error did not influence the measurement of the displacement (and therefore the potential of Wi-GIM as an early warning tool) but only of the absolute distance between nodes, which is not a meaningful parameter since it is, initially, arbitrary.

Since the network is meant to be installed in locations where a direct LOS is not always available, it was important to assess the limits of the range and inter-visibility of the nodes. Experiments showed that the nodes can efficiently communicate up to 150 m with a 360° angle of view when dense vegetation, trees and even solid objects are placed between two nodes, without affecting the precision. The Roncovetro

**Table 4**
Cost benefit table of Wi-GIM compared with RTS a GB-InSAR; a) includes the cost of the protection structure (1200€) and the reinforced concrete pillar on which the instrument is installed (400€); b) includes protection structure (2000€) and the supporting structure needed for the ground based radar (200€); c) include the cost of the SIM card (200€) and the modem necessary for data transmission (500€).

| | Costs | | | | | | | | |
|---|---|---|---|---|---|---|---|---|---|
| | Case | Nodes or targets | Direct costs | Energy consumption | Maintenance costs | Installation costs | | Data transmission costs[c] | TOT |
| | – | n. | (€) | (€) | (€) | Materials (€) | Labor (€) | (€) | (€) |
| Wi-GIM | 1 | 5 | 400 | 20 | 1500 | 0 | 200 | 700 | 2820 |
| | 2 | 30 | 2400 | 120 | 1800 | 0 | 200 | 700 | 5220 |
| RTS | 1 | 5 | 11,600 | 150 | 200 | 1600[a] | 500 | 700 | 14,750 |
| | 2 | 30 | 14,600 | 200 | 350 | 1600[a] | 700 | 700 | 18,150 |
| GB-InSAR | 1 | – | 54,000 | 300 | 100 | 2200[b] | 500 | 700 | 58,100 |
| | 2 | – | 54,000 | 300 | 100 | 2200[b] | 500 | 700 | 58,100 |

| | Benefits | | | | | | | | |
|---|---|---|---|---|---|---|---|---|---|
| | Durability | Completeness of information | Precision | Maximum range | Environmental impact | Influence of atmospheric events | | Installation effort | Mean |
| | | | | | | Rain | Snow | | |
| Wi-GIM | 2 | 4 | 2 | 2 | 3 | 4 | 4 | 5 | 3.25 |
| RTS | 3 | 5 | 4 | 5 | 4 | 3 | 3 | 3 | 3.75 |
| GB-InSAR | 5 | 3 | 5 | 5 | 4 | 4 | 1 | 4 | 3.88 |

campaign also revealed that the measurements were not affected by rain or snow.

Wi-GIM has been tested as an early warning tool to monitor very slow to rapid landslides, subsidence and tension cracks. These applications are possible due to the easy installation of the nodes, the adaptability of the network and the acquisition frequency. Automatic warnings are issued when the battery levels are low and when customizable velocity thresholds are exceeded.

The main limitations of the system are the precision (up to 2–5 cm if data are filtered and averaged) and the duration of the batteries (variable depending on air temperature, but approximately few weeks with hourly acquisition). These issues are related to the prototype nature of Wi-GIM and to the aim of using only low-cost components. They can be overcome if the system undergoes an industrialization process and as new cost-effective modules enter the market.

## Acknowledgements

This paper describes results of the project "Wi-GIM: Wireless Sensor Network for landslide monitoring and early warning" (LIFE12/ENV/IT001033) financed by Life+ Program, the EU's instrument supporting environmental, nature conservation and climate action projects throughout the EU.

## References

Abracon, 2017. http://www.abracon.com/chip-antenna/ACA-107-T.pdf, Accessed date: October 2017.

Almagià, R., 1907. Studi geografici sulle frane in Italia. Mem. Soc. Geogr. It. 13 (1) Roma.

Bertolini, G., 2010. Large earth flows in Emilia-Romagna (Northern Apennines, Italy): origin, reactivation and possible hazard assessment strategies [Große Schuttströme in Emilia-Romagna (Nördlicher Apennin, Italien): Ursache, Reaktivierung und mögliche Strategien zur Gefahrenbeurteilung]. Z. Dtsch. Ges. Geowiss. 161 (2), 139–162.

Bertolini, G., Fioroni, C., 2013. Large Reactivated Earth Flows in the Northern Apennines (Italy): an Overview. In: Landslide Science and Practice. Springer Berlin Heidelberg, pp. 51–58.

Casagli, N., Frodella, W., Morelli, S., Tofani, T., Ciampalini, A., Intrieri, E., Raspini, F., Rossi, G., Tanteri, L., Lu, P., 2017. Spaceborne, UAV and ground-based remote sensing techniques for landslide mapping, monitoring and early warning. Geoenviron. Disasters 4 (9), 1–23. http://dx.doi.org/10.1186/s40677-017-0073-1. Available at: https://geoenvironmental-disasters.springeropen.com/articles/10.1186/s40677-017-0073-1.

Cina, A., Piras, M., 2015. Performance of low-cost GNSS receiver for landslides monitoring: test and results. Geomatics Nat. Hazards Risk 6 (5–7), 497–514.

Cruden, D.M., Varnes, D.J., 1996. Landslide types and processes. In: Turner, A.K., Schuster, R.L. (Eds.), Landslides: Investigation and Mitigation. National Academy Press, Washington DC, USA, pp. 36–75.

Decawave, 2017a. https://www.decawave.com/products/dwm1000-module, Accessed date: July 2017.

Decawave, 2017b. https://www.decawave.com/sites/default/files/resources/DWM1000-Datasheet-V1.6.pdf, Accessed date: October 2017.

Dunnicliff, J., 1993. Geotechnical Instrumentation for Monitoring Field Performance. John Wiley & Sons, New York.

Dunnicliff, J., 1995. Monitoring and instrumentation of landslides. In: Bell, D.H. (Ed.), Proceedings of the Sixth International Symposium on Landslides. Christchurch. Balkema, Rotterdam, pp. 1881–1896.

Falsi, C., Dardari, D., Mucchi, L., Win, M.Z., 2006. Range estimation in UWB realistic environments. In: Proceedings of the IEEE International Conference on Communications, pp. 5692–5697.

Farina, P., Leoni, L., Babboni, F., Coppi, F., Mayer, L., Ricci, P., 2011. IBIS-M, an innovative radar for monitoring slopes in open-pit mines. In: Proc., Slope Stability 2011: International Symposium on Rock Slope Stability in Open Pit Mining and Civil Engineering, Vancouver (Canada), 18–21 September.

Fernández-Steeger, T., Arnhardt, C., Walter, K., Haß, S.E., Niemeyer, F., Nakaten, B., Homfeld, S.D., Asch, K., Azzam, R., Bill, R., Ritter, H., 2009. SLEWS—A prototype system for flexible real time monitoring of landslides using an open spatial data infrastructure and wireless sensor networks. Geotechnol. Sci. Rep. 13, 3–15.

Garich, E.A., 2007. Wireless, Automated Monitoring for Potential Landslide Hazards. M.S. thesis. Dept. Civil Eng., Texas A & M Univ., College Station, TX, USA.

Gigli, G., Intrieri, E., Lombardi, L., Nocentini, M., Frodella, W., Balducci, M., Venanti, L.D., Casagli, N., 2014. Event scenario analysis for the design of rockslide countermeasures. J. Mt. Sci. 11 (6), 1521–1530.

Gili, J.A., Corominas, J., Rius, J., 2000. Using global positioning system techniques in landslide monitoring. Eng. Geol. 55, 167–192.

Giordan, D., Allasia, P., Manconi, A., Baldo, M., Santangelo, M., Cardinali, M., Corazza, A., Albanese, V., Lollino, G., Guzzetti, F., 2013. Morphological and kinematic evolution of a large earthflow: the Montaguto landslide, southern Italy. Geomorphology 187, 61–79. ISSN 0169-555X. https://doi.org/10.1016/j.geomorph.2012.12.035.

Günther, J., Heunecke, O., Pink, S., Schuhbäck, S., 2008. Developments towards a low-cost GNSS based sensor network for the monitoring of landslides. In: Proceedings of the 13th FIG International Symposium on Deformation Measurements and Analysis, Lisbon, Portugal, 12–15.

Heunecke, O., Glabsch, J., Schuhbäck, S., 2011. Landslide monitoring using low cost GNSS equipment n experiences from two alpine testing sites. J. Civil Eng. Archit. 5 (8).

Hill, C.D., Sippel, K.D., 2002. Modern deformation monitoring: a multi sensor approach. In: Proc. FIG 22nd Int. Conf., Washington, DC, USA, Apr. 2002, pp. 1–12.

Intrieri, E., Gigli, G., Mugnai, F., Fanti, R., Casagli, N., 2012. Design and implementation of a landslide early warning system. Eng. Geol. 147-148, 124–136. http://dx.doi.org/10.1016/j.enggeo.2012.07.017. Available at: http://www.sciencedirect.com/science/article/pii/S001379521200230X.

Intrieri, E., Gigli, G., Nocentini, M., Lombardi, L., Mugnai, F., Casagli, N., 2015. Sinkhole monitoring and early warning: an experimental and successful GB-InSAR application. Geomorphology 241, 304–314. http://dx.doi.org/10.1016/j.geomorph.2015.04.018. Available at: http://www.sciencedirect.com/science/article/pii/S0169555X15002305.

Kotta, H.Z., Rantelobo, K., Tena, S., Klau, G., 2011. Wireless sensor network for landslide monitoring in Nusa Tenggara Timur. TELKOM - NIKA (Telecommun. Comput. Electron. Control) 9 (1), 9–18.

Kung, H.-Y., Hua, J.-S., Chen, C.-T., 2006. Drought forecast model and framework using wireless sensor networks. J. Inf. Sci. Eng. 22, 751–769.

Liu, D.A., Yang, Z.F., Tang, C.H., Wang, J., Liu, Y., 2004. An automatic monitoring system for the shiplock slope of Wuqiangxi Hydropower Station. Eng. Geol. 76, 79–91.

Lombardi, L., Nocentini, M., Frodella, W., Nolesini, T., Bardi, F., Intrieri, E., Carlà, T., Solari, L., Dotta, G., Ferrigno, F., Casagli, N., 2017. The Calatabiano landslide (southern Italy): preliminary GB-InSAR monitoring data and remote 3D mapping. Landslides 14 (2), 685–696.

Malet, J.P., Maquaire, O., Calais, E., 2002. The use of Global Positioning System techniques for the continuous monitoring of landslides: application to the Super-Sauze earthflow (Alpes-de-Haute-Provence, France). Geomorphology 43 (1), 33–54.

Mantovani, F., Pasuto, A., Silvano, S., Zannoni, A., 2000. Collecting data to define future hazard scenarios of the Tessina landslide. Int. J. Appl. Earth Obs. Geoinf. 2, 33–40.

Mora, P., Baldi, P., Casula, G., Fabris, M., Ghirotti, M., Mazzini, E., Pesci, A., 2003. Global positioning systems and digital photogrammetry for the monitoring of mass movements: application to the Ca'di Malta landslide (northern Apennines, Italy). Eng. Geol. 68 (1), 103–121.

Mouser, 2017. https://www.mouser.it/ProductDetail/ABRACON/ACA-107-T/?qs=eXqj2UlT4Sxq6yV1xjaQWQ%3D%3D, Accessed date: October 2017.

Ohbayashi, R., Nakajima, Y., Nishikado, H., Takayama, S., 2008. Monitoring system for landslide disaster by wireless sensing node network. In: Proc. IEEE 1st Int. Annu. Conf. SICE, Aug. 2008, pp. 1704–1710.

Petley, D.N., Mantovani, F., Bulmer, M.H., Zannoni, A., 2005. The use of surface monitoring data for the interpretation of landslide movement patterns. Geomorphology 66, 133–147.

Ramesh, M.V., Kumar, S., Rangan, P.V., 2009. Wireless sensor network for landslide detection. In: Proc. ICWN. 2009. pp. 89–95.

Read, J., Stacey, P., 2009. Guidelines for open pit slope design. CSIRO Publishing.

Rizzo, V., Leggeri, M., 2004. Slope instability and sagging reactivation at Maratea (Potenza, Basilicata, Italy). Eng. Geol. 71, 181–198.

Rosi, A., Berti, M., Bicocchi, N., Castelli, G., Corsini, A., Mamei, M., Zambonelli, F., 2011. Landslide monitoring with sensor networks: experiences and lessons learnt from a real-world deployment. Int. J. Sens. Netw. 10 (3), 111–122.

Severin, J., Eberhardt, E., Leoni, L., Fortin, S., 2014. Development and application of a pseudo-3D pit slope displacement map derived from ground-based radar. Eng. Geol. 181, 202–211.

Sheth, A., Tejaswi, K., Mehta, P., Parekh, C., Bansal, R., Merchant, S., Singh, T., Desai, U.B., Thekkath, C.A., Toyama, K., 2005. Senslide: a sensor network based landslide prediction system. In: Proceedings of the 3rd International Conference on Embedded Networked Sensor Systems, pp. 280–281.

Squarzoni, C., Delacourt, C., Allemand, P., 2005. Differential single-frequency GPS monitoring of the La Valette landslide (French Alps). Eng. Geol. 79 (3), 215–229.

Terzis, A., Anandarajah, A., Moore, K., Wang, I.-J., 2006. Slip surface localization in wireless sensor networks for landslide prediction. In: Proc. Sensor Netw. Int. Conf. Inf, pp. 109–116.

Vaziri, A., Moore, L., Ali, H., 2010. Monitoring systems for warning impending failures in slopes and open pit mines. Nat. Hazards 55, 501–515.

Win, M.Z., Scholtz, R.A., 1998. Impulse radio: how it works. IEEE Commun. Lett. 2 (2), 36–38.

Win, M.Z., Dardari, D., Molisch, A.F., Wiesbeck, W., Zhang, J., 2009. History and applications of UWB [scanning the issue]. In: Proceedings of the IEEE. 97:2. pp. 198–204.